Article type: Full Paper

High Speed and Stable Solution-processed Triple Cation Perovskite Photodetectors

*Ting Zhang, Jiang Wu, Peng Zhang, Waseem Ahmad, Yafei Wang, Mahdi Alqahtani, Hao Chen, Chunming Gao, Zhi David Chen, Zhiming Wang, Shibin Li**

Dr. Ting Zhang, Dr. Peng Zhang, Dr. Waseem Ahamd, Dr. Yafei Wang. Dr. Hao Chen, Prof. Chunming Gao, Prof. Shibin Li

School of Optoelectronic Information

University of Electronic Science and Technology of China

Chengdu, 610054, China

E-mail: shibinli@uestc.edu.cn

Dr. Jiang Wu, Mr. Mahdi Alqahtani

Department of Electronic and Electrical Engineering

University College London

Torrington Place, London WC1E 7JE, UK

Prof. Zhi David Chen

Department of Electrical & Computer Engineering and Center for Nanoscale Science & Engineering

University of Kentucky

Lexington, Kentucky 40506, USA

Dr. Jiang Wu, Prof. Zhiming Wang

Institute of Fundamental and Frontier Sciences

University of Electronic Science and Technology of China

Chengdu, 610054, China

Keywords

triple cation perovskite photodetectors, photoresponse properties, Schottky barrier, environmental stability

Abstract

Photodetectors, which can convert light signals into electrical signals, are important opto-electronic devices applied in imaging, optical communication, biomedical/biological sensing and so on. Here we demonstrate a solution-processed photodetector based on the triple cation perovskite. The perovskite photodetectors showed a high detectivity, high speed, as well as excellent environmental stability. Operating at a low voltage bias of 2 V, the photodetectors exhibited a large on/off ratio of 10^5, high specific detectivity of ~ 10^{13} Jones, and a fast photoresponse with 3 dB bandwidth up to 0.82 MHz. Further analysis demonstrates that such performance originates from the modulated Schottky barrier height by illumination. The barrier suppresses dark current without any illumination but can be effectively lower under illumination, thus resulting in a more efficient charge extraction and collection. Our results demonstrate a great potential of triple cation perovskite in photodetection, and provide a route to achieve high performance devices.

1. Introduction

Currently, commercial photodetectors (PDs) are mainly made from the inorganic semiconductor materials, including Si, ZnO, GaN, and InGaAs.[1-6] These devices show fast response and high responsitivity due to their outstanding electrical and optical properties. However, such materials are either expensive or require vacuum equipment, e.g. metal-organic chemical vapor deposition, to fabricate,[7-9] which places a restriction on a wide deployment. In recent years, organometal trihalide perovskites (OTPs) (with a structure of ABX_3, where A is an organic cation $CH_3NH_3^+$ (MA), B is Pb^{2+}, X is a halide anion or mixed halide) have drawn great attention and been a very promising candidate for opto-electronic applications due to low cost and high throughput solution process. Since the discovery of perovskite-based solar cells (PSCs) by Tsutomu Miyasaka in 2009,[10] power conversion efficiencies (PCEs) have exceeded 22% in less than seven years,[11] thanks to the outstanding physics properties, including the low exciton binding energy, strong light absorption, long carrier lifetime, large carrier diffusion coefficient, and low charge recombination rate.[12-16] These features also make the emerging perovskite materials a promising alternative to conventional semiconductors used in PDs. Indeed, solution-processed OTPs have yielded PDs with excellent device performance.[16-24]

For instance, both polycrystalline films and single crystals of OTPs have been successfully used to fabricate the narrowband and broadband photodetectors.[25-27] As one of the earliest discovered and extensively researched perovskite materials, $MAPbI_3$ has been regarded as the most potential material for PDs due to its broadband absorption and superb light sensitivity. Dong et al. reported a $MAPbI_3$-based photodetector with excellent photoconductive properties.[20] Su et al. reported a self-powered photodetector based on $MAPbI_3$, which exhibited excellent responsitivity and rapid response time for wavelength ranging from ultraviolet to visible light.[28] Chen et al. fabricated a flexible UV-Vis-NIR (ultravolte-visible-near infrared) photodetector based on $MAPbI_3$ with excellent mechanical

flexibility and durability.[18] However, some issues about this material still exist. $MAPbI_3$ tends to degrade and dissociate into MAI and PbI_2 in air.[29-31] Recent work on $FAPbX_3$ (FA: $CH_3(NH_2)_2^+$, X=I, Br, Cl) PSCs demonstrates better thermal durability than methylammonium perovskites.[31-32] However, $FAPbI_3$ has two different phases at room temperature: α-phase (desired perovskite phase) and δ-phase (photoinactive phase). Also, the α-phase perovskite of FAPbI3, which is sensitive to solvents and moisture, would turn into the undesired δ-phase in an air atmosphere.[33]

To date, the best PSCs use mixed cations and halides,[11, 34-36] e.g. $(CsPbI_3)_{0.05}[(FAPbI_3)_{0.83}(MAPbBr_3)_{0.17}]_{0.95}$. The tri-cation (Cs/MA/FA) and dual-anion (Br/I) mixed perovskite films demonstrate the structures are more stabilized and less effected by environmental factors (such as heat, moisture and solvents).[35] Motivated by the success of cesium-containing triple cation perovskites in PSCs, PDs based on the mixed cation perovskites are expected to outperform its conventional counterparts. Herein, we report on triple cation mixed perovskite PDs exhibiting a fast response, high detectivity, large photocurrent on/off ratio, and excellent stability. To the best of our knowledge, it is the first demonstration of the triple cation perovskite photodetectors. Due to the optimum bandgap and large absorption coefficient, $(CsPbI_3)_{0.05}[(FAPbI_3)_{0.83}(MAPbBr_3)_{0.17}]_{0.95}$ is particularly suitable for broadband photodetector in the UV and visible light ranges.

2. Results and Discussion

All fabrication details are given in experimental methods section. **Figure** 1(a) and Figure 1(b) show the SEM image and the absorption spectrum of a perovskite film prepared on an ITO substrate, respectively. The film, which is composed of uniform grains, is smooth and compact without any pinholes. The absorption spectrum covers a broad spectral region, 400 ~ 760 nm. It has a sharp absorption edge representing a bandgap of 1.63 eV. As schematically illustrated in Figure 1(c), the device structure of the photodetectors is a stack of glass / ITO / perovskite / gold. When the device is illuminated from ITO side (bottom electrode), charge

carriers generated by above-bandgap photons at the interface between perovskite film and ITO drift across the compact film under bias voltages; the electrons drift towards the ITO and the holes to the Au. Both carriers will be collected finally to form the output photocurrent, as shown in Figure 1(d).

To investigate whether the Cs enhances the thermal stability of mixed perovskite, we measured and compared the wavelength absorption of as-prepared perovskite samples, which were kept in different conditions. As shown in **Figure 2**(a), it is evident that the absorption of perovskite films without Cs decreases quickly after being treated by successive thermal stress. The surface degrades visibly than before (see Figure S1 in the Supporting Information). Contrarily, the triple cation mixed perovskite film remains the black color and good absorption. The XRD data in Figure 2(b) demonstrates that the MA cation perovskite material decomposed and generated PbI_2 after heating for 3 h, resulting in a distinct change in perovskite diffraction peak. However, the diffraction peak value of the triple cation perovskite film did not decrease much after being treated by successive thermal stress for 3 h. The results exhibit that the Cs-containing perovskite films are more stable and can suppress the decomposition of $MAPbI_3$ effectively.

Figure 3 shows the device characteristics of the photodetectors. The I-V curves were obtained under dark and light illumination conditions. It is evident that the photocurrent curve shows a rectification behavior, which indicates that a junction barrier exists between the ITO and perovskite films. Such a junction barrier may be attributed to a Schottky contact formed at the ITO/perovskite interface and the surface states (including surface defects, vacancies and adsorption).[37] Biased at 2 V, the device showed a dark current as low as 1.5 nA, and the photocurrent increased to 3.9 μA with the illumination intensity of 0.05 mW/cm^2 using a 635 nm LD light source (see **Figure 3**a and 3b). The high photocurrent gives a high on/off ratio (rectification ratio) larger than 10^3 under a bias of 2 V. To further test the photoresponse behavior of the photodetector, photocurrents were measured under different incident light

intensities ranging from 0.05~3.5 mW/cm^2, as shown in Figure 3c. Photocurrent increases linearly with the increasing incident light intensity, indicating low recombination loss of photogenerated carries in the device. Upon light irradiation, the photocurrent increased sharply, and then decreased rapidly when the light was turned off. Figure S2 (Supporting Information) shows that the device exhibits a reproducible photocurrent response to periodic on/off light after being exposed to light illumination over 2000 s. With a high power irradiation of 3.5 mW/cm^2, the light-switching on/off ratio can be as high as 10^5 while the photocurrent reaches around 140 μA at a bias of 2 V. The results demonstrate high photo-sensitivity and capability of detecting light signal of low intensity.

Figure 3(d) shows the EQE spectra at different biases. The EQE value increased with increasing bias and can reach up to 300% measured at a bias of 10 V, due to the fact that excess charges were injected by the electrodes under applied bias voltages, except for the photogenerated charges. Moreover, the EQE curves agree well with the absorption curve (shown in Figure 1(b)). Specific responsivity was calculated and plotted in Figure 3(e). It is observed that the responsivity monotonously increases with the increasing applied bias. With the applied bias voltages at 6 V, the EQE values exceed 100%, and the corresponding responsivities are superior to Si PD ($<$0.2 A/W) even at ultraviolet wavelength regions.[38] As a result, we obtained a higher responsivity of 1.63 A/W at a bias of 10 V for our device.

To further characterize the performance of PDs, specific detectivity (D*) is analyzed. Assuming dark current is the main contribution to the total noise, D*can be expressed as: $D^* = \frac{R}{\sqrt{(2qJ_d)}}$, where J_d is the dark current density. Figure 3(f) shows the detectivity curves measured at different bias. D* under -1 V and -2 V were calculated to be above 10^{12} and 10^{13} Jones (Jones = cm × Hz$^{\frac{1}{2}}$ × W^{-1}) respectively. The high detectivity value means that weak light signals can be detected and transferred into large electrical signals. At 0 V, D* is

measured as high as 10^{14} Jones. A smaller J_d mainly ascribes to the low thermal emission rates and high perovskite film quality, both of which prevent large leakage current.

Another important figure of merit for photodetectors is the response speed, which can be defined as the time spent on the initial current to increase to 90% of the peak output value, or vice versa. We used an oscilloscope to record the temporal response. In **Figure 4**(a), the rise time and decay time for our device are extracted to be 19 and 84 μs, respectively. The fast response time is primarily determined by the charge transport and collection, which would be strongly affected by the electronic trap states existing at the interface of semiconductor/metal. It is observed that the decay time shows a slower decay rate. An interpretation for such a phenomenon is possible presence of surface states which keep photo-carriers from immediate collection or recombination after switching off illumination.[19] Finally, we measured the response of our detector to a pulsed LD light at different frequencies. Figure 4(b) depicts the curve of normalized response versus light pulse frequency, showing the −3 dB bandwidth (f_{-3dB}) is 0.82 MHz. The bandwidth is larger than that of the reported photodetectors based on a bulk perovskite single crystal and perovskite nanowires.[24, 27] To compare the device reported in this work to the state-of-the-arts, the performance of perovskite-based photodetectors are briefly summarized in **Table** 1. In comparison with the previous works, the simple photodetector demonstrated excellent performance in all aspects, including EQE (317%), responsivity (1.63 A/W), detectivity (>10^{13} Jones), and rise/decay time (1.9×10^{-5}/8.4×10^{-5} s).

The energy band diagram (see in **Figure 5**) of our device under dark and illumination conditions was plotted to gain an insight into the high device performance. Although the energy level diagram of $(CsPbI_3)_{0.05}[(FAPbI_3)_{0.83}(MAPbBr_3)_{0.17}]_{0.95}$ has never been pictured in the past, an approximate energy positions of valence and conduction bands for the triple cation perovskite can be estimated using the energy levels of three different perovskites,[49-50] as shown in Figure 5(a). Considering the optical absorption band edge, we estimated the CBM

(conduction band minimum) of triple cation perovskite should be much higher than that of $FAPbI_3$, and the VBM (valence band maximum) of triple cation perovskite is slightly higher than that of $FAPbI_3$, as shown in Figure 5(b). Under zero bias voltage and no illumination, the device is in an equilibrium state and the band alignment is shown in Figure 5(c), of which φ_B means the Schottky barrier height. Specifically, due to charge transfer after bringing the ITO electrode in contact with the perovskite film, a depletion layer would be formed near the surface of perovskite film. As a result of the band bending, a Schottky barrier is formed at the ITO/ perovskite interface. Both the depletion layer and the space charge region have been proved to be helpful in separating photoexcited charge carriers. When the device is under bias voltages and illumination, as shown in Figure 5(d), the strong local electric field acting on Schottky barrier area will separate the photogenerated holes and electrons quickly and reduce the hole-electron recombination rate, leading to an increase of free carrier density. The increased free carrier density would lower the effective Schottky barrier height by changing the Femi level, thus resulting in the easier tunneling and transport for carriers. In other words, photogenerated electrons would inject into the ITO electrode and the holes would move to the gold contact, as schematically depicted in Figure 5(d) and Figure 1(d). Once the light illumination is turned off, the carrier recombination will increase quickly that reduce the free carrier density greatly, resulting in a significantly increased Schottky barrier height.

To check the environmental stability of our photodetector, we measured the photocurrent response of a device upon illumination with a 635 nm light (0.05 mW cm^{-2}) after being storeed for one week in ambient conditions with 35~45% relative humidity (see Figure S3, Supporting Information). Notably, our device showed nearly consistent photocurrent response, indicating good environmental stability. In comparison, the responsivity of a $MAPbI_3$-based photodetector stored under the same conditions decreased rapidly and significantly and after one day, no obvious photocurrent can be detected.[13]

Figure 6 shows the triple-cation perovskite device characteristics after being stored for two months in ambient conditions with 35~45% relative humidity. To compare and evaluate a device lifetime, the measurement is under the same conditions as before (illuminated with a 0.05 mW cm^{-2} 635 nm light and biased at 2 V). Comparing the curves of dark current, photocurrent, EQE and responsivity, a negligible change is observed after being stored for two months under the above-mentioned conditions. Such small changes could be resulted from experimental run-to-run errors. The results imply our device has a good long-term environmental stability. Figure 6d depicts the rise and decay time for our device kept for two months. The extracted values are 25 and 95 μs, respectively, which are slightly larger than the response time of initial device but remain the same order of magnitude. Therefore, the triple cation perovskite-based photodetectors can resist humidity penetration and oxygen degradation effectively, as evidenced from the consistent device performance after being used and kept in ambient air for extended time.

3. Conclusion

In summary, we present triple cation perovskite-based photodetectors that can be applied to broadband spectrum detection in this work. The device with a simple configuration shows excellent performance, which is comparable to or even better than $MAPbI_3$-based photodetectors. Operating at a bias of 2 V, the as-prepared photodetectors exhibited a large light on/off ratio of 10^5 upon illumination with 635 nm light, high specific detectivity (~ 10^{13} Jones), 3 dB bandwidth (0.82 MHz), as well as good environmental stability (>2 months). Such an excellent photoresponse property is related to the Schottky barrier formed by the contact of ITO/ perovskite; it would be effectively lower when illuminated, thus resulting in more efficient charge extraction and collection. This work demonstrates a great potential of triple cation perovskite in opto-electronic detection, and provides a promising route to achieve high performance.

4. Experimental Section

Synthesis and Characterization of triple cation perovskite: Indium tin oxide (ITO) substrates were cleaned by acetone, ethyl alcohol and deionized (DI) water with each step for 15 min. After that, the substrates were further treated by UV ozone. The mixed perovskite precursor solutions were prepared by mixing 1 M (mol/L) FAI, 1.1 M PbI_2, 0.2 M MABr and 0.2 M $PbBr_2$ in anhydrous DMF: DMSO (4:1 v/v). After stirring for 12 h, 1.5 M CsI (pre-dissolved in DMSO) was add into the mixed perovskite solutions with a volume ratio of 5:95 to obtain the desired composition of triple cation perovskite. All the early-stage preparations were carried in a nitride-filled glove box. The morphologies of as-prepared films were measured by field emission scanning electron microscopy (FE-SEM). X-ray diffraction (XRD) patterns were recorded using an X-ray diffractometer (Cu Kα radiation, λ=1.54056 Å) to study the crystal quality of the perovskite films. The ultraviolet-visible (UV-Vis) absorption spectra were measured using a UV-Vis spectrophotometer (Shimadzu UV-3101 PC).

Fabrication of the photodetectors: The precursor solution was spin-coated by two-steps: 1000 and 5000 rpm for 10 s and 40 s, respectively. At the last 5 s of the coating, 200 µl of chlorobenzene was added to the substrate. Films turned dark immediately after this treatment. The substrates were then annealed at 100℃ for 1 h in a nitrogen-filled glovebox. Finally, gold electrodes with a thickness of 80 nm as the back contact were deposited by thermal evaporation. For each device, the photoactive area defined by the electrode was 0.04 cm^2.

Photoresponse Measurements: The typical current - voltage characteristics of the devices were measured using a Keithley 4200 Semiconductor Parametric Analyzer under the illumination of a 635 nm LD light. Photocurrent with on/off cycles were measured with an oscilloscope (Agilent DOS5012A) and an optical chopper modulating the light illuminated on the device. External quantum efficiencies and responsitivities were characterized by a QE-R measurement system equipped with a calibrated Si PD as the reference (Enli tech from

Taiwan). All the measurements were performed at room temperature in the ambient atmosphere.

Supporting Information

Figure S-1. The optical images of perovskite films after being treated by successive thermal stress for 3 h at 130°C in dry air.

Figure S-2. A reproducible I-t curve of the device measured for periodic light on/off.

Figure S-3. Comparison of environmental stability of the device kept in air for one week with 35~45% relative humidity.

Acknowledgements

This work was supported by National Natural Science Foundation of China under Grant Nos. 61421002, 61474015, 61574029, 61471085 and 61371046. This work was also partially supported by University of Kentucky.

References

[1] L. Wang, J. Jie, Z. Shao, Q. Zhang, X. Zhang, Y. Wang, Z. Sun, S.-T. Lee, *Adv. Funct. Mater.* **2015**, *25*, 2910.

[2] M. Otto, M. Algasinger, H. Branz, B. Gesemann, T. Gimpel, K. Füchsel, T. Käsebier, S. Kontermann, S. Koynov, X. Li, V. Naumann, J. Oh, A. N. Sprafke, J. Ziegler, M. Zilk, R. B. Wehrspohn, *Adv. Opt. Mater.* **2015**, *3*, 147.

[3] T. Zhang, B. Liu, W. Ahmad, Y. Xuan, X. Ying, Z. Liu, Z. Chen, S. Li, *Nanoscale Res. Lett.* **2017**, *12*, 522.

[4] Y. Jin, J. Wang, B. Sun, J. C. Blakesley, N. C. Greenham, *Nano Lett.* **2008**, *8*, 1649.

[5] D. Fan, K. Lee, S. R. Forrest, *ACS Photonics*, **2016**, *3*, 670.

[6] X. Wang, J. Song, P. Li, J. H. Ryou, R. D. Dupuis, C. J. Summers, Z. L. Wang, *J. Am. Chem. Soc.* **2005**, *127*, 7920.

[7] X. Gong, M. Tong, Y. Xia, W. Cai, J. S. Moon, Y. Cao, G. Yu, C.-L. Shieh, B. Nilsson, A. J. Heeger, *Science*, **2009**, *325*, 1665.

[8] K.-J. Baeg, M. Binda, D. Natali, M. Caironi, Y.-Y. Noh, *Adv. Mater.* **2013**, *25*, 4267.

[9] Y. Guo, C. Liu, H. Tanaka, E. Nakamura. *J. Phys. Chem. Lett.* **2015**, *6*, 535.

[10] A. Kojima, K. Teshima, Y. Shirai, T. Miyasaka, *J. Am. Chem. Soc.* **2009**, *131*, 6050.

[11] W. S. Yang, B. W. Park, E. H. Jung, N. J. Jeon, Y. C. Kim, D. U. Lee, S. S. Shin, J. Seo, E. K. Kim, J. H. Noh, S. I. Seok, *Science*, **2017**, *356*, 1376.

[12] T. Leijtens, S. D. Stranks, G. E. Eperon, R. Lindblad, E. M. J. Johansson, I. J. McPherson, H. Rensmo, J. M. Ball, M. M. Lee, H. J. Snaith, *ACS nano*, **2014**, *8*, 7147.

[13] X. Gu, Y. Wang, T. Zhang, D. Liu, R. Zhang, P. Zhang, J. Wu, Z. D. Chen, S. Li, *J. Mater. Chem. C*, **2017**, *5*, 10754.

[14] S. Li, P. Zhang, Y. Wang, H. Sarvari, D. Liu, J. Wu, Y. Yang, Z. Wang, Z. D. Chen, *Nano Res.* **2017**, *10*, 1092.

[15] D. Liu, S. Li, P. Zhang, Y. Wang, R. Zhang, H. Sarvari, F. Wang, J. Wu, Z. Wang, Z. D. Chen, *Nano Energy,* **2017**, *31*, 462.

[16] M. I. Saidaminov, M. A. Haque, J. Almutlaq, S. Sarmah, X.-H. Miao, R. Begum, A. A. Zhumekenov, I. Dursun, N. Cho, B. Murali, O. F. Mohammed, T. Wu, O. M. Nakr, *Adv. Opt. Mater.* **2017**, *5*.

[17] H. Wang, D. H. Kim, *Chem. Soc. Rev.* **2017**, *46*, 5204.

[18] S. Chen, C. Teng, M. Zhang, Y. Li, D. Xie, G. Shi, *Adv. Mater.* **2016**, *28*, 5969.

[19] V. Adinolfi, O. Ouellette, M. I. Saidaminov, G. Walters, A. L. Abdelhady, O. M. Bakr, E. H. Sargent, *Adv. Mater.* **2016**, *28*, 7264.

[20] R. Dong, Y. Fang, J. Chae, J. Dai, Z. Xiao, Q. Dong, Y. Yuan, A. Centrone, X. C. Zeng, J. Huang, *Adv. Mater.* **2015**, *27*, 1912

[21] X. Hu, X. Zhang, L. Liang, J. Bao, S. Li, W. Yang, Y. Xie, *Adv. Funct. Mater.* **2014**, *24*, 7373.

[22] Y. Wang, Y. Zhang, Y. Lu, W. Xu, H. Mu, C. Chen, H. Qiao, J. Song, S. Li, B. Sun, Y.-B. Cheng, Q. Bao, *Adv. Opt. Mater.* **2015**, *3*, 1389.

[23] X. Li, D. Yu, J. Chen, Y. Wang, F. Cao, Y. Wei, Y. Wu, L. Wang, Y. Zhu, Z. Sun, J. Ji, Y. Shen, H. Sun, H. Zeng, *ACS Nano*, **2017**, *11*, 2015.

[24] W. Deng, L. Huang, X. Xu, X. Zhang, X. Jin, S.-T. Lee, J. Jie, *Nano Lett*, **2017**, *17*, 2482.

[25] L. Dou, Y. M. Yang, J. You, Z. Hong, W.-H. Chang, G. Li, Y. Yang, *Nat. Commun.* **2014**, *5*, 5404.

[26] M. I. Saidaminov, M. A. Haque, M. Savoie, A. L. Abdelhady, N. Cho, I. Dursun, U. Buttner, E. Alarousu, T. Wu, O. M. Bakr, *Adv. Mater.* **2016**, *28*, 8144.

[27] Y. Fang, Q. Dong, Y. Shao, Y. Yuan, J. Huang, *Nat. Photonics*, **2015**, *9*, 679.

[28] L. Su, Z. X. Zhao, H. Y. Li, J. Yuan, Z. L. Wang, G. Z. Cao, G. Zhu, *ACS Nano*, **2015**, *9*, 11310.

[29] Y. Han, S. Meyer, Y. Dkhissi, K. Weber, J. M. Pringle, U. Bach, L. Spiccia, Y.-B. Cheng, *J. Mater. Chem. A*, **2015**, *3*, 8139.

[30] P. Zhang, J. Wu, Y. Wang, H. Sarvari, D. Liu, Z. D. Chen, S. Li, *J. Mater. Chem. A*, **2017**, *5*, 17368.

[31] G. E. Eperon, S. D. Stranks, C. Menelaou, M. B. Johnston, L. M. Herz, H. J. Snaith. *Energy Environ. Sci.* **2014**, *7*, 982.

[32] J.-W. Lee, D.-H. Kim, H.-S. Kim, S.-W. Seo, S. M. Cho, N.-G. Park, *Adv. Energy Mater.* **2015**, *5(20)*.

[33] C. Yi, J. Luo, S. Meloni, A. Boziki, N. Ashari-Astani, C. Grätzel, S. M. Zakeeruddin, U. Röthlisberger, M. Grätzel, *Energy Environ. Sci.* **2016**, *9*, 656.

[34] Y. Wang, J. Wu, P. Zhang, D. Liu, T. Zhang, L. Ji, X. Gu, Z. D. Chen, S. Li, *Nano Energy*, **2017**, *39*, 616.

[35] M. Saliba, T. Matsui, J.-Y. Seo, K. Domanski, J.-P. Correa-Baena, M. K. Nazeeruddin, S. M. Zakeeruddin, W. Tress, A. Abate, A. Hagfeldt, M. Grätzel, *Energy Environ. Sci.* **2016**, *9*, 1989.

[36] T. Ye, S. Ma, X. Jiang, L. Wei, C. Vijila, S. Ramakrishna, *Adv. Funct. Mater.* **2017**, *27*, 1606545.

[37] H. Kind, H. Yan, B. Messer, M. Law, P. Yang, *Adv. Mater.* **2002**, *14*, 158.

[38] F. Guo , B. Yang , Y. Yuan , Z. Xiao , Q. Dong , Y. Bi , J. Huang, *Nat. Nanotechnol.* **2012**, *7*, 798.

[39] H. Deng, X. Yang, D. Dong, B. Li, D. Yang, S. Yuan, K. Qiao, Y.-B. Cheng, J. Tang, H. Song, *Nano Lett.* **2015**, *15*, 7963.

[40] Y. Zhang, J. Du, X. Wu, G. Zhang, Y. Chu, D. Liu, Y. Zhao, Z. Liang, J. Huang, *ACS Appl. Mater. Interfaces*, **2015**, *7*, 21634.

[41] H. Deng, D. Dong, K. Qiao, L. Bu, B. Li, D. Yang, H.-E. Wang, Y. Cheng, Z. Zhao, J. Tang, H. Song, *Nanoscale*, **2015**, *7*, 4163.

[42] C. Ma, Y. Shi, W. Hu, M.-H. Chiu, Z. Liu, A. Bera, F. Li, H. Wang, L.-J. Li, T. Wu, *Adv. Mater.* **2016**, *28*, 3683.

[43] J. Song, L. Xu, J. Li, J. Xue, Y. Dong, X. Li, H. Zeng, *Adv. Mater.* **2016**, *28*, 4861.

[44] M. I. Saidaminov, V. Adinolfi, R. Comin, A. L. Abdelhady, W. Peng, I. Dursun, M. Yuan, S. Hoogland, E. H. Sargent, O. M. Bakr, *Nat. Commun.* **2015**, *6*.

[45] L. Shen, Y. Lin, C. Bao, Y. Bai, Y. Deng, M. Wang, T. Li, Y. Lu, A. Gruverman, W. Li, J. Huang, *Mater. Horiz.* **2017**, *4*, 242.

[46] F. Li, C. Ma, H. Wang, W. Hu, W. Yu, A. D. Sheikh, T. Wu, *Nat. Commun.* **2015**, *6*.

[47] Y. Lee, J. Kwon, E. Hwang, C.-H. Ra, W. J. Yoo, J.-H. Ahn, J. H. Park, J. H. Cho, *Adv. Mater.* **2015**, *27*, 41.

[48] D.-H. Kang, S. R. Pae, J. Shim, G. Yoo, J. Jeon, J. W. Leem, J. S. Yu, S. Lee, B. Shin, J.-H. Park, *Adv. Mater.* **2016**, *28*, 7799.

[49] C.-C. Chueh, C.-Z. Li, A. K.-Y. Jen, *Energy Environ. Sci.* **2015**, *8*, 1160.

[50] Y. G. Kim, T.-Y. Kim, J. H. Oh, K. S. Choi, Y.-J. Kim, S. Y. Kim, *Physical Chemistry Chemical Physics*, **2017**, *19*, 6257.

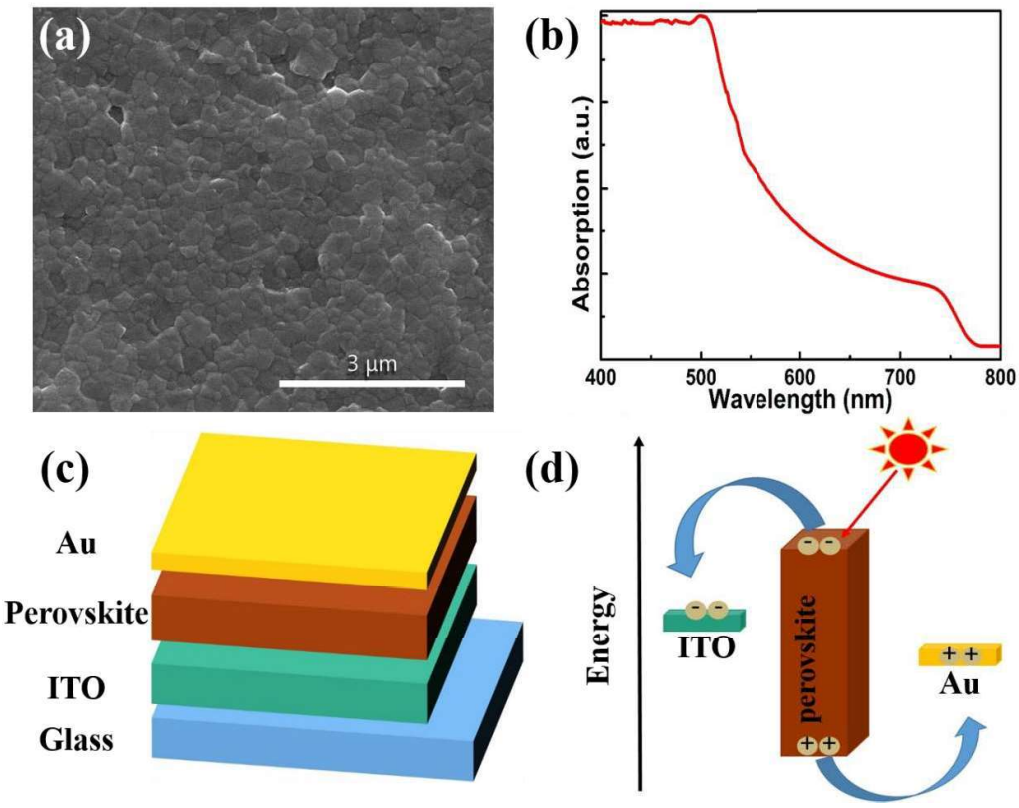

Figure 1. (a) Top view SEM image and (b) Absorption spectra of the perovskite film. (c) Schematic of the triple cation mixed perovskite photodetector. (d) Schematic diagram of charge carrier transfer in the device under illumination.

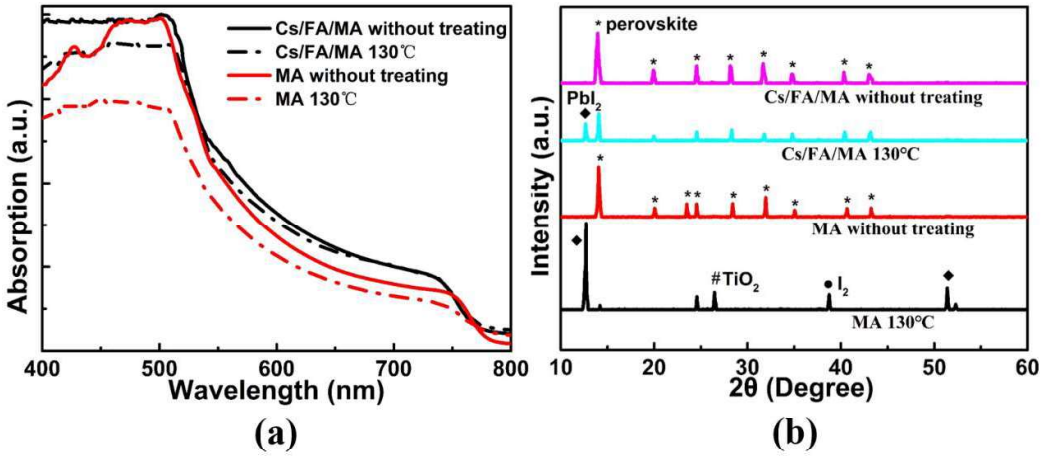

Figure 2. (a) Optical absorption and (b) XRD data of triple cation mixed perovskite and $MAPbI_3$. The treating process means perovskite films were annealed at 130°C for 3 hours in dry air.

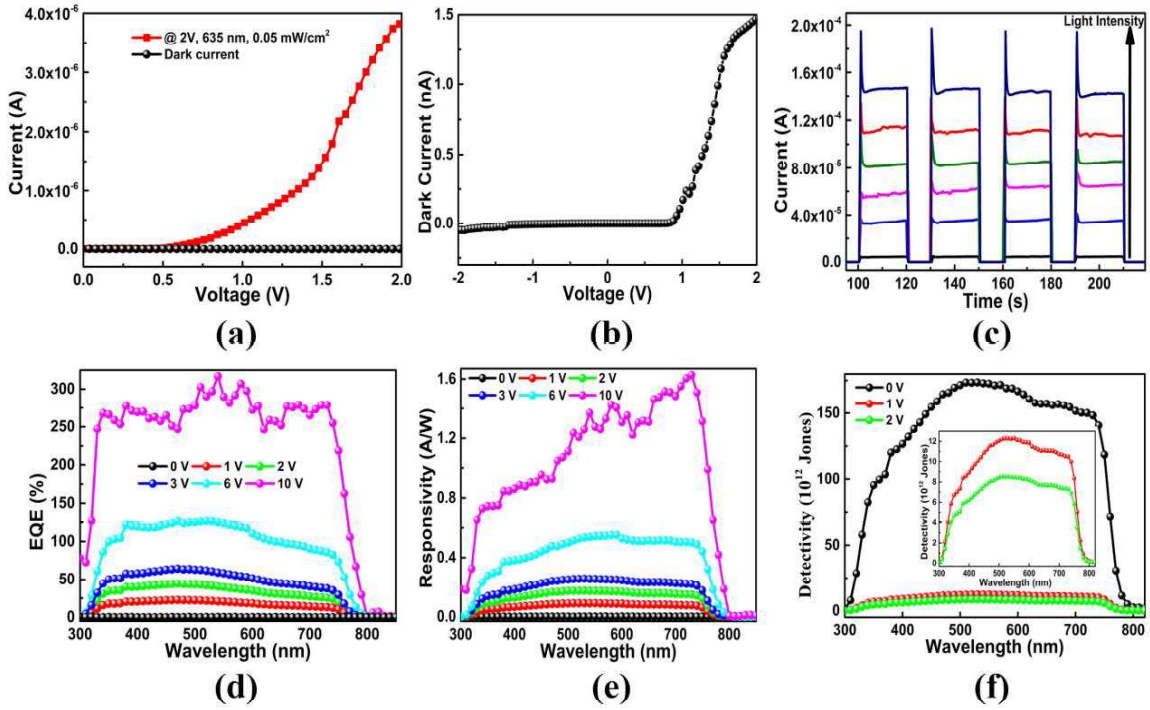

Figure 3. (a) I-V curves of the device in the dark and under illumination with light intensity of 0.05 mW/cm^2 (635 nm light source) at 2 V. (b) Zoomed-up dark current curve. (c) I-t curves of the PD under bias voltage of 2 V at different light intensities (635 nm light source). (d) EQE and (e) Responsivity spectra under different biases. (f) Specific detectivities of our photodetector under different biases. The insert is an enlarged portion of D^* at -1 and -2 V.

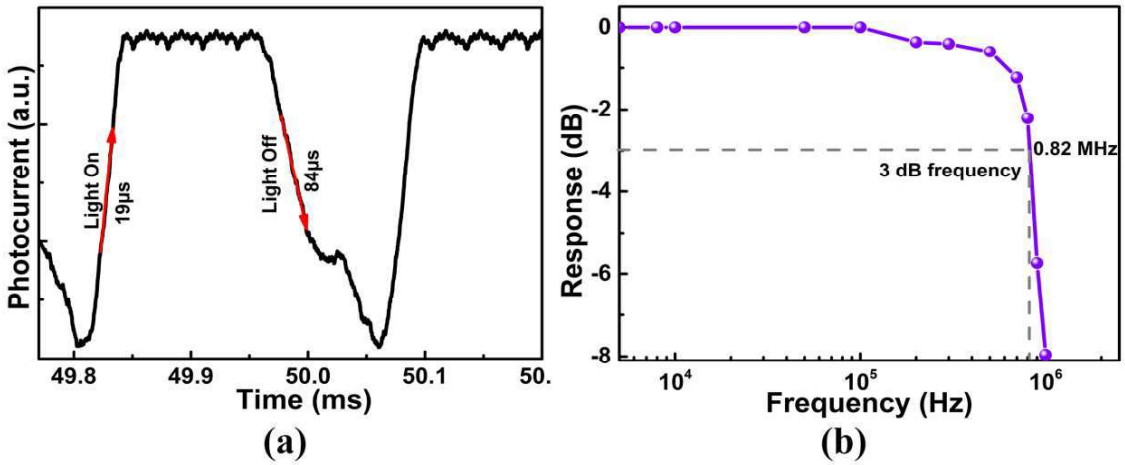

Figure 4. (a) Transient photocurrent response of our detector at a frequency of 20 KHz. (b) Normalized photoresponse as a function of light frequency, showing a 3 dB bandwidth of 0.82 MHz.

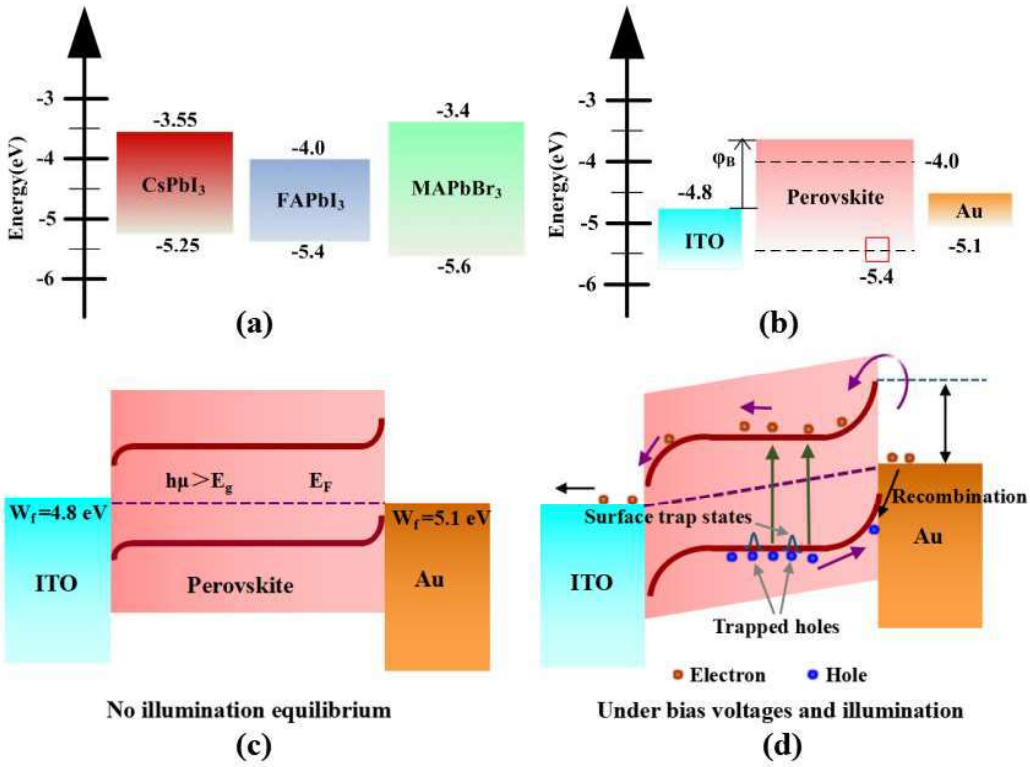

Figure 5. (a) Band diagram of $CsPbI_3$, $FAPbI_3$, $MAPbBr_3$. (b) Band diagram for the triple cation perovskite device. Schematic illustrations of band structure for our device (c) under zero bias voltage in the dark and (d) under bias voltages and illumination. Upon illumination, the lower Schottky barrier height leads to photogenerated holes move to the surface and are trapped by the surface trap states, leaving behind more unpaired electrons move to the electrode, resulting in a great increasement of photocurrent and photoresponse.

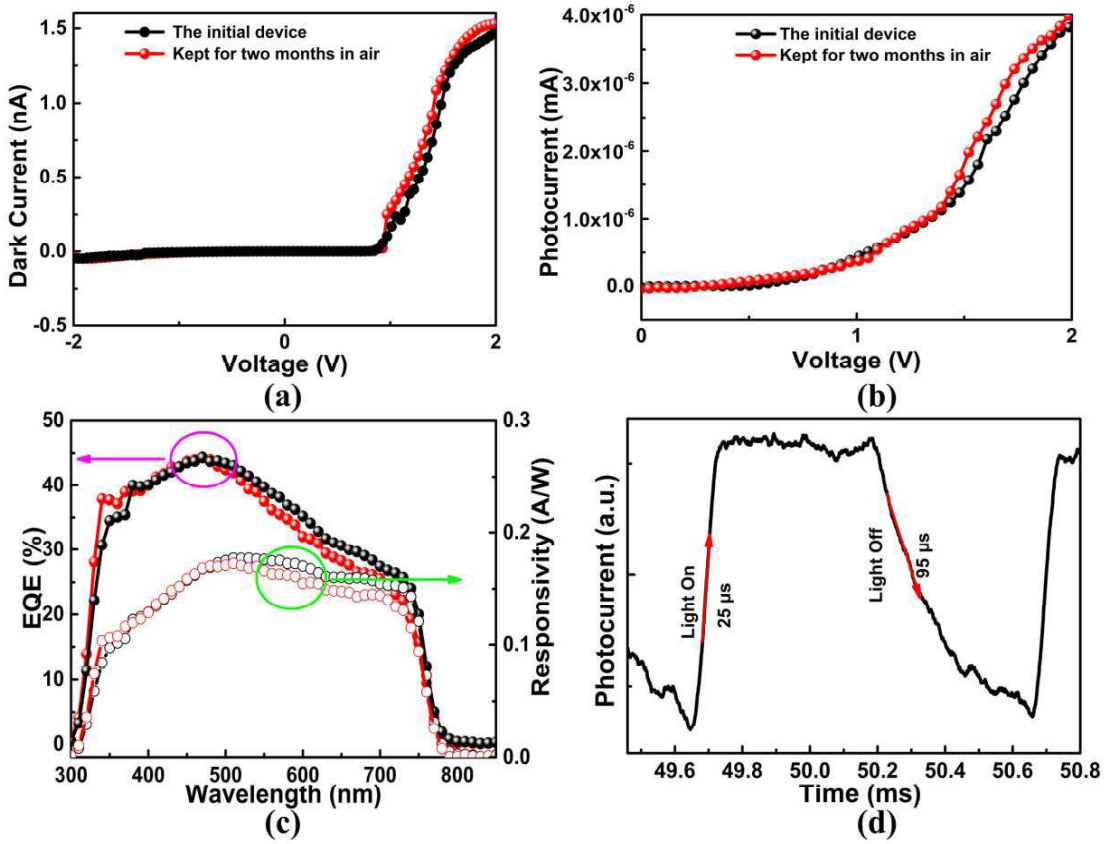

Figure 6. Opto-electronic performance of our photodetectors kept for two months in ambient air. I-V curves of the device (a) In the dark and (b) Under illumination with light intensity of 0.05 mW/cm^2 (635 nm light source) at 2 V. (c) EQE and Responsivities spectra biased at 2 V. Black represents EQE and responsivity of the initial device. Red means these parameters of the device measured after keeping for two months in ambient air. (d) Transient photocurrent response of our detector at a frequency of 5 KHz.

Table 1. Performance comparison of our photodetector with other reported photodetectors based on perovskites.

Materials structure	Configurations	EQE (%)	Responsivity (A/W)	Detectivity (Jones)	Rise/ decay time (ms)	Refs.
Triple cation mixed perovskite film	Photoconduction	317	1.63	~10^{13}	0.019/0.084	Our work
$MAPbI_3$ film	Photoconduction	1190	3.49	-	~100/100	[21]
$MAPbI_3$ network	Photoconduction	-	0.1	1.02×10^{12}	0.3/0.4	[39]
$MAPbI_3$ island	Photoconduction	-	-	-	~40/50	[40]
$MAPbI_3$ NW arrays	Photoconduction	-	12500	1.73×10^{11}	0.00034/0.00042	[24]
$MAPbI_3$ NW arrays	Photoconduction	-	1.3	2.5×10^{12}	0.2/0.3	[41]
$MAPbI_3$ crystal	Photoconduction	2×10^{5}	1604	~10^{13}	~0.03/0.02	[26]
$MAPbI_3$+PDPP3T film	Photoconduction	~10	0.05	8.8×10^{10}	40/140	[18]
$MAPbI_3$+WS_2 film	Photoconduction	-	17	2×10^{12}	2.7/7.5	[42]
$CsPbBr_3$ nanosheets	Photoconduction	54	0.64	-	0.019/0.024	[43]
$MAPbI_3$ film	Photodiode	-	14.5	-	0.0002/0.0007	[9]
$MAPbI_{3-x}Cl_x$ film	Photodiode	80	-	~10^{14}	1.6×10^{-4}	[25]
$MAPbBr_3$ crystal	Photodiode	-	4000	＞10^{13}	-/0.025	[44]
$MAPbI_3$+PDPPTDTPT film	Photodiode	~75	-	＞10^{11}	5×10^{-6}	[45]
$MAPbI_3$ film	phototransistor	~80	320	-	0.0065/0.005	[46]
$MAPbI_3$+graphene film	phototransistor	5×10^{4}	180	＞10^{9}	87/540	[47]
$MAPbI_3$+MoS_2 film	phototransistor	-	1.94×10^{6}	1.29×10^{12}	6170/4500	[48]

High speed and stable solution-processed triple cation perovskite photodetectors are demonstrated. To date, the best perovskite solar cells use mixed cations and halides. However, the triple cation perovskite photodetectors have never been reported. Except for the excellent photoresponse properties, the triple cation perovskite photodetectors show a good environmental stability compared with the reported perovskite-based photodetectors.

Keyword:

triple cation perovskite photodetectors, photoresponse properties, Schottky barrier, environmental stability

High Speed and Stable Solution-processed Triple Cation Perovskite Photodetectors